AERO-THERMAL RE-ENTRY SENSITIVITY ANALYSIS USING DSMC AND A HIGH DIMENSIONAL MODEL REPRESENTATION-BASED APPROACH

Alessandro Falchi, Edmondo Minisci, Massimiliano Vasile, and Martin Kubicek

Aerospace Centre of Excellence (ACE), University of Strathclyde

James Weir Building, 75 Montrose St, Glasgow G1 1XQ. UK

Emails: {alessandro.falchi, edmondo.minisci, massimiliano.vasile, martin.kubicek}@strath.ac.uk

ABSTRACT

This paper presents a sensitivity analysis for the hypersonic aero-thermal convective heat transfer from the free molecular to the slip-flow regime for cylindrical and cubic geometries. The analyses focus on a surface-averaged heat transfer coefficient at various atmospheric conditions. The sensitivity analyses have been performed by coupling a High Dimensional Model Representation-based approach and a Direct Simulation Monte Carlo code. The geometries have been tested with respect to different inputs parameters; altitude, attitude, wall temperature and geometric characteristics. After the initial sensitivity analyses, the N-dimensional surrogate models of the surface-averaged heat transfer coefficient have been defined and tested. Hereby, a shape-based DSMC mesh refinement correction factor for reducing the overall analyses computational times is also presented.

Key words: DSMC; Heat Transfer; Sensitivity Analysis; Re-entry Analysis; Surrogate Modeling.

1. INTRODUCTION

Aero-thermal re-entry analyses are of utmost importance when design for demise and spacecraft or satellites survivability analyses are pursued. Indeed, in accordance with the NASA-STD-8719.14, every satellite or space structures, whose end of life is expected to end with an uncontrolled re-entry must satisfy the Human Casualty Risk requirements. To assess the re-entry survivability and the related human casualty risk, different software may be used, such as DAS (Debris Assessment Software [8]) and ORSAT (Object Reentry Survival Analysis Tool [12]) maintained by NASA, or SCARAB (Spacecraft Atmospheric Reentry and Aerothermal Breakup [6]) currently used by the European Space Agency.

An object re-entering the atmosphere passes through different flow regimes, each with a decreasing rarefaction degree: Free Molecular Flow (FMF), transitional, slip-flow, and continuum regime. Different high fidelity tools such as DSMC and CFD may be applied at the appropriate regime, even though they can be very computationally expensive. Most low-fidelity tools that model the ablation of re-entering spacecraft are based on the hypersonic panel method, which provides reasonable aero-thermal results for hemispherical objects, but fail to characterize cubic or sharp-edged objects. In addition, the theories are valid only within the continuum regime under the hypersonic flow condition. The low-fidelity models can provide reliable results within the FMF regime by using analytical models [15]. Characterizing and investigating the transitional and slip flow regime would provide the opportunity to generate more accurate bridging functions [10].

The aim of this work is to reliably quantify the sensitivity of input parameters over the heat transfer phenomena within the transitional and slip-flow regime. The analyses have been performed with the dsmcFoam software [13]. This study is focused on the characterization of averaged heat transfer coefficients of a cube and a flat cylinder. Defining the local surface heat transfer coefficient as in eq. 1:

$$C_H = \frac{2\dot{Q}}{\rho V_\infty^3} \tag{1}$$

Where ρ is the mass density, V_∞ is the free flow velocity and $\dot{Q}$ is the convective heat flux.

The surface-averaged heat transfer coefficient ($\widetilde{C}_H$), which has been considered for the sensitivity analysis, for each DSMC simulation is computed by reading the object surface's heat flux, as defined in eq. 2:

$$\widetilde{C}_H = \frac{\sum_{i=1}^{N_f} C_{H,i} \cdot A_i}{\sum_{i=1}^{N_f} A_i} \tag{2}$$

Where N_f is the total number of surface mesh facets, A_i is i-th facet area, and $C_{H,i}$ is the i-th facet heat transfer as defined in eq. 1.

Initially, six different parameters had been deemed as possibly influent: Knudsen number (Kn, strictly related to the altitude), attitude side-slip (α) and angle of attack (β), free-flow relative velocity (V_∞), Wall temperature (T_{wall}), geometric scaling factor (for the cube) and the length to radius ratio (L/R, for the cylinder).

Since DSMC analyses are very computationally expensive when performed within the transitional regime, two different approaches have been applied to reduce the overall computational cost of the analyses but yet maintaining a high level of accuracy. The first method consists on the employment of the efficient adaptive derivative HDMR algorithm [7], which defines the number of samples required to evaluate the N-Dimensional independent variables' domain depending on the complexity of the analyzed function. The second approach is based on the characterization of a corrective coefficient that would allow to greatly reduce the DSMC computational times by exploiting a correlation between different levels of mesh refinements, i.e.: mean free path (λ) to cell size ratio and particles per cell (PPC). A correction factor (C_F) as a function of the Knudsen number has been defined for each analyzed geometry.

After the sensitivity analysis, which defines the most influencing parameters on the heat transfer phenomenon, the surrogate model (SM) of the $\widetilde{C}_H$ for the considered objects has been defined. The aim is to implement the SM within the Free Open Source Tool for Re-entry of Asteroids and Debris[9] (FOSTRAD) for accurately characterizing the FMF to continuum regime bridging functions. Such SM would improve FOSTRAD aero-thermal module in the transitional regime re-entry phase, allowing an accurate characterization of the surface-averaged aero-thermal heating. Indeed, the SM defined for parameterized geometries would be easy to implement and fast to evaluate, making the tool suitable for studying simple shaped objects ablation employing a lumped-mass approach.

In the first part of Section 2, a brief description of the DSMC and simulation inputs is given, while the characterization of the mesh-refinement corrective coefficient is presented in the second part. Section 3 focuses on the application of the DSMC and HDMR code and their coupling. The sensitivity analyses results are shown in Section 4. The elaboration and application of $\widetilde{C}_H$ SMs are presented in Section 5.

2. DSMC SETUP AND MESH REFINEMENT CORRECTION FACTOR

A general and short description of DSMC setup, boundary conditions, and simulation inputs is presented in this section. In addition, the method used to decrease the DSMC computational times is explained.

Table 1. Cube (L_{ref} = 1m) Aero-thermodynamic heating DSMC inputs.

ID	Name	Min	Central	Max
1	Kn	0.08	5.04	10
2	$\alpha[deg]$	0	22.5	45
3	$\beta[deg]$	0	22.5	45
4	$V_\infty[m/s]$	-	7600	-
5	$T_{wall}[K]$	350	875	1400
6	Scale	0.75	1	2

2.1. dsmcFoam And Simulations Inputs

The DSMC simulations have been performed using the dsmcFoam [13] solver implemented within the Computational Fluid Dynamic (CFD) toolbox OpenFOAM. The tool allows the computation of convective heat transfer of arbitrary three-dimensional geometries. The geometries have been handled by using the *snappyHexMesh* tool, which creates the flow-field polyhedral unstructured mesh and the extruded layers on the surface explicit geometry. The dsmcFoam tool has been validated for non-reacting and reacting flows, for which it employs a Quantum-Kinetic chemistry model [14]. The collision statistical computation and post-collision energy distribution are evaluated via the Larsen-Borgnakke variable hard sphere (VHS) model [2]. For the investigation, a fully diffusive reflective wall boundary condition has been employed.

This paper focuses on the heat transfer computation within the transitional and slip-flow regime, the atmospheric inputs have been obtained from the Naval Research Laboratory Mass Spectrometer and Incoherent Scatter Radar Exosphere[11] (NRLMSISE-00) model. The cube has been simulated by taking into account 6 different parameters (Table 1): Knudsen, side-slip angle and angle of attack (respectively α and β), free flow relative velocity (V_∞), wall temperature (T_{wall}) and a linear geometric scaling factor. A preliminary investigation had shown that the velocity variation within an arbitrarily chosen interval (6800$\div$8400m/s) has a negligible impact over the $\widetilde{C}_H$, therefore, a fixed value has been used for the performed HDMR analysis. The input for the cylinder investigation are reported in table 2. For this case, the velocity has not been considered, and it had been set constant at 7600m/s. In addition, by taking advantage of the symmetric shape, only the side-slip angle has been considered. Moreover, it has been investigated the influence of the length to radius ratio (L/R, at a constant radius) instead of investigating the $\widetilde{C}_H$ variation due to a scaling factor.

All the flow properties such as mass density, 5 atomic densities (O, O_2, N, N_2, Ar), and free flow temperature are determined in accordance to the simulated Kn and

Table 2. Cylinder (R = 0.25m, L_{ref} = 0.5m) Aerothermodynamic heating DSMC inputs.

ID	Name	Min	Central	Max
1	Kn	0.08	5.04	10
2	$\alpha[deg]$	0	45	90
3	$T_{Wall}[K]$	350	875	1400
4	L/R	0.2	1	1.5

the reference length of the simulated object. The Kn is defined as in Eq. 3.

$$Kn = \frac{\lambda}{l_{ref}} \tag{3}$$

Where λ is the free flow mean free path and l_{ref} is the reference length. For a VHS model λ is defined [1, 4] as in Eq. 4 :

$$\lambda_{VHS} = \left(\frac{2\mu}{15}\right)(7-2\omega)(5-2\omega)\frac{1}{\rho\sqrt{2\pi RT_\infty}} \tag{4}$$

Where μ is the real gas viscosity, ω is the viscosity coefficient temperature exponent, ρ is the mass density, R is the specific gas constant and T_∞ is the free flow temperature. It is evident that expressing the altitude as a function of Kn is not straightforward. The evaluation is performed numerically by employing an atmospheric database.

In order to have accurate results, DSMC simulations must be performed by using a mesh whose average cell size (C_x) is a fraction of λ (Eq. 5):

$$C_x = \frac{\lambda}{MFPR} \tag{5}$$

where MFPR is the mean free path to cell size ratio, which is commonly recommended to be set within $2 \div 3$ [16]. Another secondary parameter which may affect the simulation accuracy is the number of PPC, which should be set within $10 \div 40$, a higher PPC is generally associated with a higher accuracy and computational cost. Therefore, the mesh resolution is dependent on the λ and so also on the Kn and altitude. This represents the biggest limitations of the DSMC method, in fact, as the flow regime approaches the continuum, the mean free path increases exponentially, thus, the simulations become computationally too expensive to be feasible. In addition, having a mesh resolution that must be dependent on the λ leads to the necessity of having a "Knudsen-adaptive" mesh. This is a critical phase of the investigation, indeed, the mesh must be properly defined in order to allow

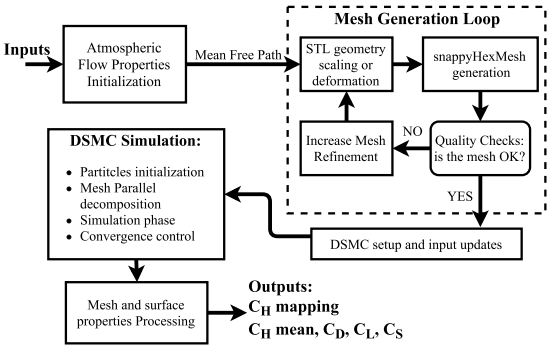

Figure 1. DSMC Simulation process flowchart.

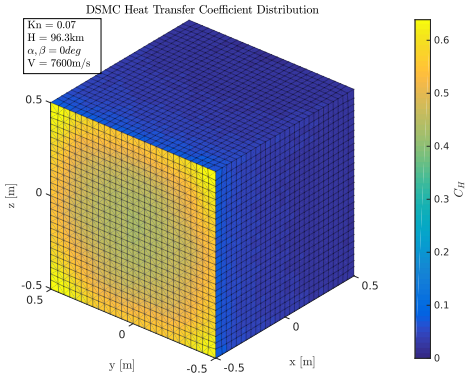

Figure 2. DSMC Heat transfer coefficient Surface distribution over a cube at a hypersonic slip-flow regime condition, resulting from the automated simulation process shown in Figure 1.

the automated post-processing phase. On top of that, the complexity of the problem is increased by the fact that the transitional regime simulations are very computationally expensive and must be parallel-processed, meaning that also the mesh decomposition must be handled with care to prevent mesh-based glitches. Moreover, the simulations must be processed on a mesh which has been layered on the simulated geometry. The snappyHexMesh tool layer generation phase is highly dependent on the geometry, and because the layering could influence the results, a set of automated checks had to be performed on the mesh quality before initializing each simulation. A simplified flowchart for the DSMC simulation process is presented in Figure 1. A resulting C_H surface distribution is shown for the two geometries in the figures 2 and 3.

2.2. DSMC High-Low fidelity Correction Factor

During this work, the possible correlation between the "high-fidelity"(HF) DSMC simulation results to "low-fidelity"(LF) ones has been investigated, as this would save a massive amount of computational time. The results have been deemed as promising, and are hereby pre-

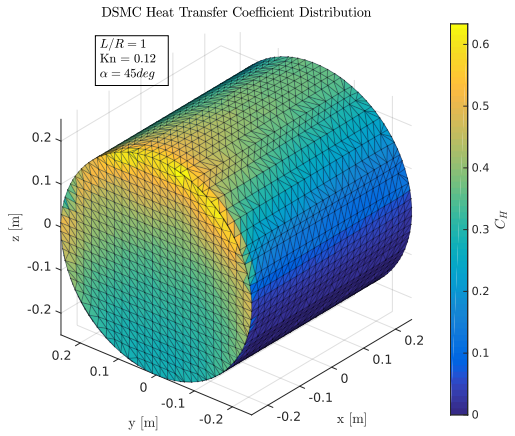

Figure 3. DSMC Heat transfer coefficient Surface distribution over a cube at a hypersonic transitional regime flow condition. Directly obtained during the correction factor definition phase.

sented. The two different fidelity levels have been defined as:

- High-fidelity simulation: MFPR = 3; PPC = 40
- Low-fidelity simulation: MFPR = 1; PPC = 10

Assuming that the computational cost of a DSMC simulation depends solely on the number of cells (which is proportional to the number of particles and collision computation), and even by neglecting the computational time required by the mesh generation phase, it has been seen that the computational time of a DSMC simulation is approximately $T_{comp} \propto 1/C_x^3$. Thus, at a constant atmospheric condition and altitude (i.e.: constant λ), the computational time increases proportionally to the cube of the $MFPR$. Therefore, a simulation running with a HF setup, even if neglecting the difference in the PPC, would cost $\sim$27 times more than a LF computation.

As an example, consider a simulation that had been run at Kn = 0.05 on an object with a l_{ref} = 0.5m using a MFPR = 1 and so a $C_x = \lambda = 0.025$m. The simulation had required more than 8M cells and a $T_{comp} \simeq 2800$core-hours for reaching a good degree of convergence. The same simulation with a MFPR = 3 would have required more than 70000 core-hours, which is equivalent to 10 days of run-time on 288cores.

By establishing a preliminary correction factor (C_F) as a function of Kn and the attitude, the correlation between the surface-averaged results of HF and LF aerodynamic and aero-thermodynamic coefficients such as drag, lift, and heat transfer was deemed as possible. In this work, only the correlation of the average heat transfer has been used. Defining the C_F as the ratio between the HF and LF averaged properties (Eq. 6):

Table 3. Configurations evaluated for defining the C_F.

Case	Kn Range	Attitudes
Cube	0.11$\sim$10	$\alpha = \beta = [0; 45]deg$
Cylinder	0.12$\sim$10	$\alpha = [0; 45; 90]deg$

$$C_F = \frac{\widetilde{C}_{H,HF}}{\widetilde{C}_{H,LF}} \tag{6}$$

Where $\widetilde{C}_{H,HF}$ and $\widetilde{C}_{H,LF}$ are respectively the surface-averaged heat transfer coefficients obtained by using the HF and LF DSMC setup. A correlation defined in such way would inevitably lead to an error, whose evaluation should be done also taking into account the computational time that could be potentially saved. In order to define a C_F, a minimum number of evaluations of the HF setup must be performed, therefore, the approach is computationally cost-efficient when a high number of simulations is expected. It must be reminded that the method is characterized by the intrinsic limitation of being representative of surface averaged properties, therefore, the uncertainty of the defined C_F would be higher if applied for estimating the local surface properties. Even though the C_F is based on the mesh refinement, it must be reminded that a minimum amount of cells is required to accurately capture the object geometry. In fact, an altered surface geometry will inevitably cause errors in the results. Therefore, since the number of particles has a low influence on the accuracy, the C_F would be sensibly differing from the unity when $\lambda/MFRP$ drops below a predefined "maximum FMF cell size", which happens at a Kn* based on the object's reference length.

The C_F has been studied according to the attitudes and Kn ranges reported in Table 3. All the other simulations' inputs had been set at their central values (Tables 1 and 2). In Figures 4-5 the $\widetilde{C}_H$ for the two geometries is shown. For the cube, it is possible to notice that the $\widetilde{C}_H$ begins to diverge for $Kn < 0.75$ In fact, for higher Kn the maximum cell size is limited by the object geometry resolution, therefore, the HF and LF C_x is the same. An analogous behavior is shown for the cylinder (Figure 5), even though the divergence begins at a slightly lower Kn, which is dependent on the l_{ref} and mesh resolution setup. The $\widetilde{C}_H$ estimated by the LF DSMC simulations is higher than the HF one. In addition, the trend is the same at different attitudes for both geometries. The C_F (Figures 6-7) show that the difference between the HF and LF simulations increases as the Kn decreases. In addition, the C_F function has a step-like shape, which is caused by the rounded discrete number of cells used to build the flow-field mesh.

Observing the cube analyses, the C_F values at the two extreme attitude $\alpha = \beta = [0; 45]deg$ show a maximum

Table 4. $\widetilde{C}_{H,LF}$ standard deviation (σ) for the cube at α,β = 45deg.

Kn	1	0.75	0.5	0.25	0.20
σ [$\cdot 10^{-3}$]	0.31	0.25	0.25	0.26	0.23

difference around $\sim 4\%$. Therefore, even by using a C_F as a function of Kn, linearly weighted on the attitude (or an equivalent projected area), would result into an error which is deemed as acceptable. Especially if it is considered the computational time that the C_F application would save. During this study, the potential impact of a higher uncertainty on the LF DSMC simulations has also been studied. By running a set of 35 simulations at constant and different Kn, a relatively small standard deviation (σ <1E-3, Table 4) has been shown for the $\widetilde{C}_{H,LF}$.

The cylindrical shape C_F has been investigated at three different attitudes: α = [0, 45, 90]deg at L/R = 1. It has been found out that the maximum $\widetilde{C}_H$ among the studied shape, occurs at α = 45deg. It has been observed that the C_F at 90deg falls within the range of the other two evaluated cases, as that also happens for the $\widetilde{C}_H$.

Since the HDMR analyses were performed in within the Kn interval of [0.08; 10], the C_F have been extended to the minimum HDMR analyzed Kn = 0.08. The C_F predicted values for both geometries are shown by the interpolated lines in the Figures 6-7. In order to apply the C_F it has been used a dataset built via a piecewise cubic Hermite interpolation[3] over the Kn. For the cube HDMR simulation, the C_F has been weighted on the attitude angles. Meanwhile, considering the results of the DSMC simulations required for defining the cylindrical shape C_F, it has been decided to use a simplified $\widetilde{C}_F$ averaged between the C_F obtained at 0 and 45deg as a function of Kn (red dashed line in Figure 7). In the same figure, the σ_{C_F} error bars are also shown. The error bars are based on the C_H fluctuations observed in the preliminary simulations.

3. HDMR-DSMC APPLICATION

The Adaptive Derivative High Dimensional Model Representation [7] (AD-HDMR) is based on a cut-HDMR model and adaptive sampling. By deriving the cut-HDMR approach in a different way, and using the conclusions obtained from the derivation of the cut-HDMR approach, a new interpolation process has been defined. The algorithm flow chart could be simplified in an iterative loop mainly structured in 5 steps:

1. Decomposition of the stochastic sampling domain into sub-domains according to cut-HDMR approach

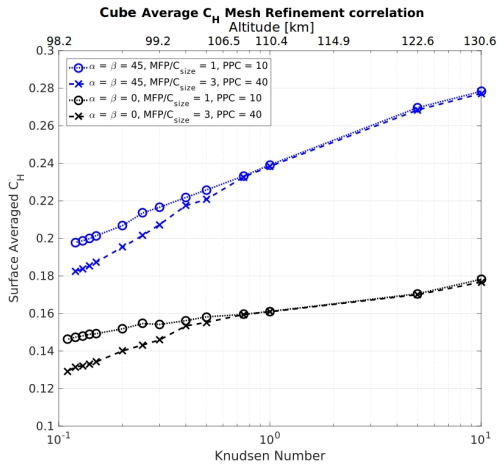

Figure 4. Surface-averaged C_H for the cube at LF and HF mesh refinement over Kn at different attitudes.

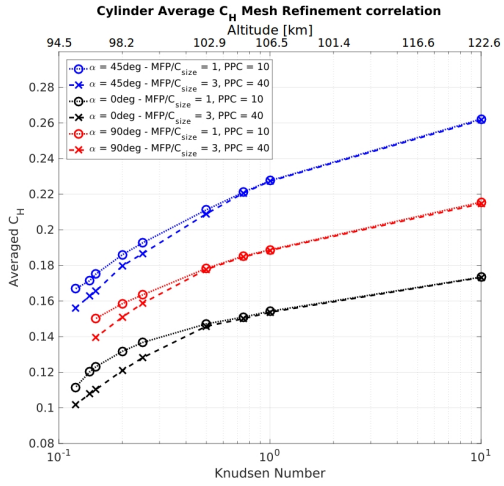

Figure 5. Surface-averaged C_H for the cylindrical geometry at LF and HF mesh refinement over Kn at different attitudes.

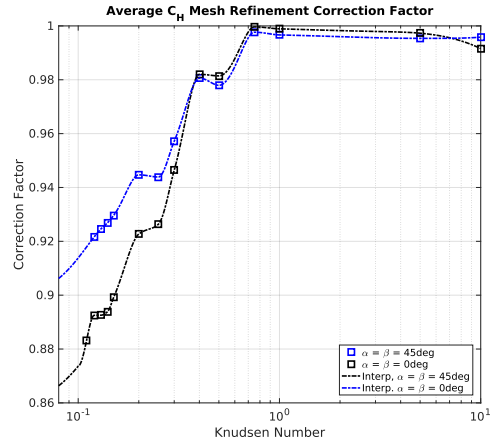

Figure 6. $\widetilde{C}_H$ Correction factor for the cube, calibrated at different Kn and attitudes.

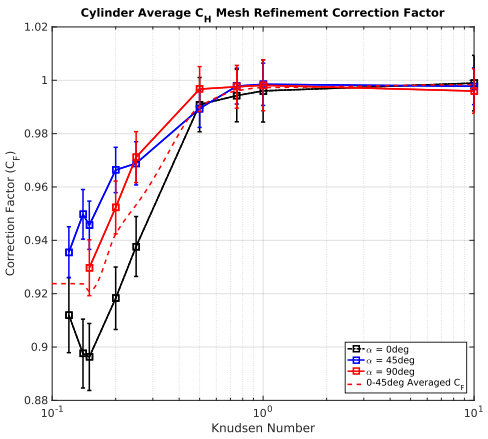

Figure 7. Cylindrical geometry correction factor for the $\widetilde{C}_H$ over Kn at different attitudes. The error bar show the maximum and minimum range from the sampled point according to $\pm 3\ \sigma_{C_F}$.

2. Selection of important stochastic sub-domains
3. Adaptive sampling
4. Function evaluations
5. Adaptive interpolation

The AD-HDMR defines when all important stochastic sub-domains are properly described and interpolated by using a user-defined convergence edge. The algorithm defines an N-dimensional SM of the evaluated function, which in this case is the $\widetilde{C}_H$. The $\widetilde{C}_H$ SM (identified as $\widetilde{\mathbb{C}}_{\mathbb{H}}$) is generated by evaluating the contribution of each one of the single input variables and their significant interactions. Using the Monte Carlo sampling on the obtained SM, statistical properties of the investigated problem can be established. Therefore, the application of the algorithm provides the following outputs:

- SM within the investigated ranges e.g.:
  $\widetilde{\mathbb{C}}_{\mathbb{H}} = f(Kn, \alpha, \beta, T_{wall}, V_{\infty}, scale)$
- Sensitivity Analysis
- Uncertainty Quantification

The coupling between the HDMR and dsmcFoam has been controlled via MATLAB on the ARCHIE-WeSt high-performance computer. Even though the C_F has been employed for limiting the computational expense of each simulation, the minimum cell size within the chosen Kn and scale factors ranges was in the order of 0.04m. Meanwhile, the flow field was in the order of 5x5x5m, which was scaled accordingly to the scale factor, and considering the object wall mesh refinement, more than 3M cells and 30M particles were generated. Such a number of cells and subsequent particles requires the use of HPC.

4. HEAT TRANSFER SENSITIVITY ANALYSIS RESULTS DISCUSSION

The adaptive HDMR algorithm has been successfully integrated with the predefined C_F for both cube and cylinder. For the cube study case, the HDMR evaluated a set of 36 DSMC simulations, which required a computational time of 206core-hours (equivalent to $\sim$26h in an 8-cores PC). For the cylindrical shape, the HDMR simulation has been run by using two different levels of convergence accuracy on the adaptive sampling. The lowest convergence edge has been reached in 40 simulations, with a total duration of 76core-hours. With the more strict convergence, the method had evaluated 72 DSMC simulations which required 132core-hours. The sensitivity analysis results list the following indexes:

- Partial Mean is the mean of the variable's $\widetilde{C}_H$ SM uniform distribution
- Partial Variance is the variance associated with each variable
- Sensitivity Mean represents the sensitivity index on deviation from the mean value, it is based on the partial mean value.
- Sensitivity Variance it is the most important index to understand the weight of the variable's SM. It is representative of the maximum or minimum deviation of the increment function for the relative variable from the zero-value. A small sensitivity variance mean that the input is negligible.
- Var(iable) Significance represents the input's weight compared to the raw error distribution (σ_{C_H}). The input is considered negligible if its maximum or minimum increment function value was comparable to the raw DSMC $\widetilde{C}_H$ error. The Variable significance edge was set at 90%.

4.1. HDMR Cube Results

The Table 5 reports the cube results for the HDMR sensitivity analysis of $\widetilde{C}_H$ by employing the weighted C_F. It has been shown that the most significant variable is the Kn and the attitude. It is interesting to notice the differences in the sensitivity of the two angles; this is due to the rotation order. The Figure 8 shows the sampled points with respect to the central values and the relative SMs. The x-axis shows each normalized variable in the interval of [0÷1], the shown interval limits corresponds to each input's minimum and maximum value reported in Table 1. It must be noted that the cube geometric scale affects the l_{ref}, therefore, a smaller cube will be simulated at a lower altitude for an equal Kn.

Table 5. Cube - HDMR sensitivity analysis results on the $\widetilde{C}_H$. The $\widetilde{C}_H$ central value is equal to 0.2453.

Input	Partial Mean	Partial Variance	Sensitivity Mean	Sensitivity Variance	Var Significance
Kn	-0.0069	0.0004	0.3758	0.4091	100%
α	-0.0043	0.0003	0.2365	0.3457	100%
β	-0.0066	0.0002	0.3593	0.231	100%
T_{wall}	0.0002	0	0.0082	0.0033	99.89%
Scale	0	0	Neglected	Neglected	33.16%
Kn-β	0.0002	0	0.0131	0.0052	100%
Kn-α	0.0001	0	0.0071	0.0058	100%

Table 6. Cylinder - HDMR sensitivity analysis results on the $\widetilde{C}_H, \delta = 0.015$. The $\widetilde{C}_H$ central value is equal to 0.2505.

Input	Partial Mean	Partial Variance	Sensitivity Mean	Sensitivity Variance	Var Significance
Kn	-0.0069	0.0003	0.1679	0.1491	100%
α	-0.0246	0.0006	0.5938	0.2629	100%
T_{wall}	-0.0004	0	0.0085	0.0025	100%
L/R	0.009	0.0003	0.2179	0.1256	100%
α-L/R	-0.0005	0.001	0.012	0.4599	100%

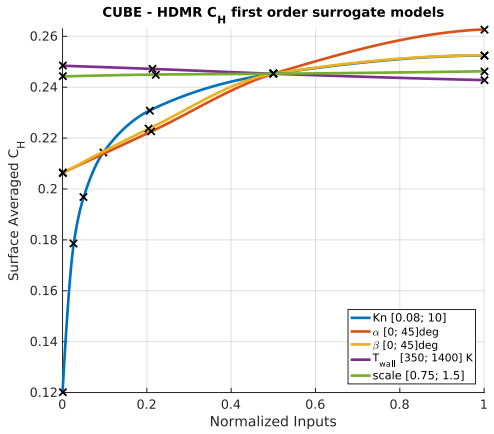

Figure 8. Cube HDMR First Order $\widetilde{\mathbb{C}}_{\mathbb{H}}$. The results are shown on a normalized x-axis, in the legend are reported the relative minimum and maximum values associated to the interval [0∼1].

4.2. HDMR Cylinder Results

As the cylinder was simulated using two different levels of convergence accuracy, the results showing the refinement effect on the N-dimensional sampling domain have been reported. Indeed, the adaptive algorithm evaluates where the functions need to be refined to test potential discontinuities. In Figure 9 the two different refined SM are reported, where δ is defined as the maximum convergence residual acceptable by the HDMR algorithm. It must be highlighted how the shape of the increment functions is better identified as δ decreases. In fact, the algorithm successfully manages to identify the points where the SM's local derivative changes and applies a local refinement of the sampling domain. It must also be reminded that the algorithm has been originally implemented for non-stochastic functions, which is not the case. Indeed, small fluctuations in the function evaluation may cause a redundancy in the sampling domain refinement. It is possible to observe these events for the L/R SM around 0.12 and for the α SM in the neighborhood of 0.2 in Figure 9.

In Table 6, the resulting sensitivity analysis for the cylinder at the finest level of convergence is reported. It is interesting to notice that for this case, the Kn is not the input with the highest sensitivity on the $\widetilde{C}_H$. Instead, the attitude and the geometrical L/R parameter have a very high sensitivity index. In addition, it is worth noting the very high sensitivity on the variance of the $\alpha - L/R$ interaction term, which is representative of the maximum and mini-

mum deviation from the $\widetilde{C}_H$ central value. Therefore, the interaction between the L/R and the side-slip angle is not negligible. In figure 10, it is shown the 3rd order polynomial SM built for the interaction increment function, which is the contribution of the interaction to the global $\widetilde{\mathbb{C}}_{\mathbb{H}}$ estimated value.

4.3. HDMR $\widetilde{C}_H$ Results Discussion

The HDMR-based heat transfer analysis on the cube has shown that small variations of the cube's scale [0.75m÷1.5m] do not influence the average heat transfer. In addition, also the T_{wall} has shown a small influence on the $\widetilde{C}_H$. The interactions between Kn and the attitude have a low variance sensitivity index as well, meaning that neglecting the two interactions would cause minor errors, which can be considered within the error induced by the introduction of the C_F. Therefore, with the perspective of using the SM within a low-fidelity tool such as FOSTRAD, it would be possible to use a SM based only on Kn, α and β.

The results on the cylindrical shape, have highlighted the same result as the cube: the T_{wall} sensitivity index is roughly the same. Therefore, the T_{wall} may be considered negligible also for the cylinder. In addition, the cylinder has shown a high mean sensitivity on the L/R ratio. Assuming that the scale would not affect the $\widetilde{C}_H$, it is possible to generate a SM which is representative of any cylinder parameterized by the length to radius ratio within the analyzed interval i.e.: $L/R \in [0.2; 1.5]$. Seen the influence on the variance sensitivity, it is paramount to use also the interaction between L/R and α. Therefore, the arbitrarily-shaped cylinder SM would be defined as a function of α, Kn, and L/R.

Focusing the attention on the $\widetilde{\mathbb{C}}_{\mathbb{H}}$ as a function of Kn in a semilogarithmic scale, it has been possible to notice a principle of convergence. Therefore it had been decided to simulate some additional samples to better capture the FMF regime for both the cube and the cylinder at Kn = [50; 100; 1000]. The extended $\widetilde{\mathbb{C}}_{\mathbb{H}}$ is shown in Figure 11. As it would have been expectable from the FM theory[5] at the two different limits of the analyzed Kn interval and moving toward the FMF or continuum regime, the $\widetilde{C}_H$ variation seems to be developing an asymptotic behavior. This result would allow the use of the SM to define a bridging function between the continuum and FMF regime which could be easily implemented in FOSTRAD.

5. HEAT TRANSFER SURROGATE MODELS APPLICATION

In order to show the resulting $\widetilde{\mathbb{C}}_{\mathbb{H}}$, different iso-parameter surfaces have been modeled for both the cube and the cylindrical shape on the most influencing parameters. An extension of the cube $\widetilde{\mathbb{C}}_{\mathbb{H}}$, which has been generated taking advantage of the geometric symmetry, is shown in Figure 12. For the cube, the SM defined only by the single influencing variables, i.e. Kn, α, β, and T_{wall} has been used. The generation of the entire dataset used for the plot required a computational time in the order of $\sim 0.05s$. In this case, the SMs of the interactions have not been used, even though their implementation would have been feasible. It has been chosen not to use the interaction surrogate models as this would introduce a higher uncertainty due to the polynomial surface fitting. Since their sensitivity variance is very small, it has been deemed that the error introduced by the approximation of the surface fitting would have been higher than the error induced by neglecting the interactions.

In Figure 13 the cylindrical geometry extended SM is shown. It is interesting to notice how the $\widetilde{\mathbb{C}}_{\mathbb{H}}$ surface shape changes as the cylinder changes from being "stocky" to being "slender". This peculiarity highlights the importance of taking into account interaction between $\alpha - L/R$ in the SM. Indeed, this behavior would not have been predicted by a SM based only on the single variables. In addition, the T_{wall} influence on the $\widetilde{C}_H$ is shown to be almost negligible (Figure 14), as it had been predicted by the Sensitivity Variance index reported in Table 6.

In order to test the quality of the cylindrical geometry complete SM, 66 DSMC simulation with randomly generated inputs within the validity ranges have been run. Defining the error as in Eq. 7:

$$Error_{\%} = \frac{C_{H_{DSMC}} - \widetilde{\mathbb{C}}_{\mathbb{H}}}{\widetilde{\mathbb{C}}_{\mathbb{H}}} \cdot 100 \tag{7}$$

It has been seen that on the average, the $\widetilde{\mathbb{C}}_{\mathbb{H}}$ underestimates the $\widetilde{C}_H$. The average percentage error is Err_{mean} = 0.839%, while the standard deviation is σ_{err} = 1.351%. The results are shown in Figure 15. Considering the computational efficiency of the surrogate model application, its implementation within a low-fidelity tool is deemed to be acceptable.

6. CONCLUSIONS

The proposed research has highlighted which parameters are most influential on the surface averaged heat transfer within the transitional regime, quantifying an index of sensitivity for each of the preliminarily selected parameters within a predefined range (sensitivity variance in tables 5-6). For two different general and parameterized geometries, the most important variables have been reported to be the attitude, altitude (expressed in terms of Knudsen number), aspect ratio (such as the length to radius ratio of the cylinder), and the interactions among these parameters. In addition, small variations of the geometric scale factor for a cube have been identified as not

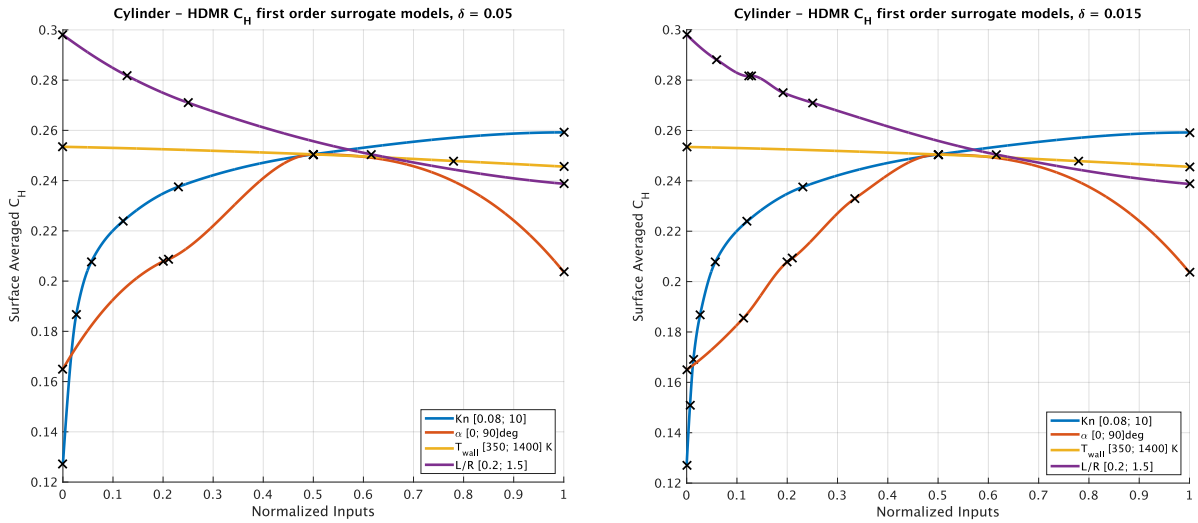

Figure 9. Cylinder HDMR single variables $\widetilde{\mathbb{C}}_{\mathbb{H}}$. The results are shown on a normalized x-axis, in the legend are reported the relative minimum and maximum values associated to the interval [0∼1]. ***On the left:*** *rough convergence $\delta = 0.05$.* ***On the right:*** *refined convergence $\delta = 0.015$.*

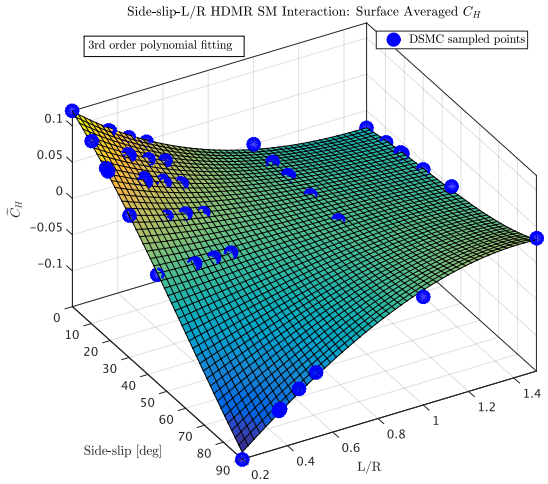

Figure 10. Cylinder: increment function SM for the interaction between the side-slip angle and L/R geometric factor. In blue are shown the $\widetilde{C}_H$ raw sampled points, the other variables are kept at their central values 2.

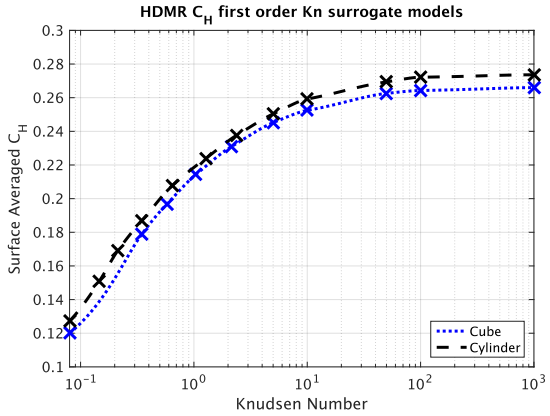

Figure 11. Cube and Cylinder $\widetilde{C}_H$ HDMR Knudsen number surrogate models extended to the free molecular regime.

influencing over the heat transfer. It must be reminded that the simulations were performed at a defined Knudsen number, therefore, the altitude was adjusted to match the input Kn and reference length, which changed according to the scale.

The surrogate models for the two analyzed shapes have been defined and are ready to be implemented within the Free Open Source Tool for Re-entry of Asteroids and Debris (FOSTRAD) for better characterizing the aero-thermal heating transitional regime bridging functions. To ensure a correct application of the surrogate models hereby defined, they will have to be used in accordance with the predefined inputs and the originally evaluated range (tables 1-2).

Alongside the primary objective of this work, a shape-

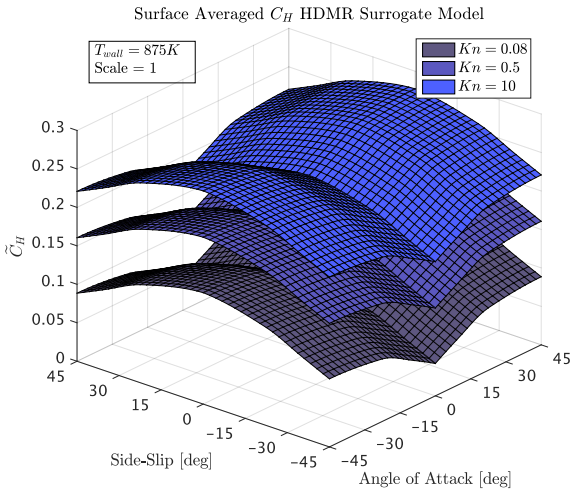

Figure 12. Cube $\widetilde{\mathbb{C}}_{\mathbb{H}}$ iso-surfaces for Kn, generated by extending the dataset to a wider range of α and β by employing the symmetry condition.

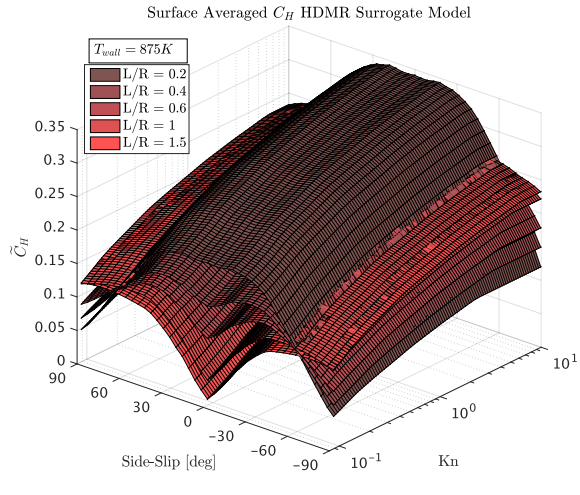

Figure 13. Cylinder $\widetilde{\mathbb{C}}_{\mathbb{H}}$ iso-surfaces for L/R, generated by extending the dataset to a wider range of α by employing the axial-symmetry condition.

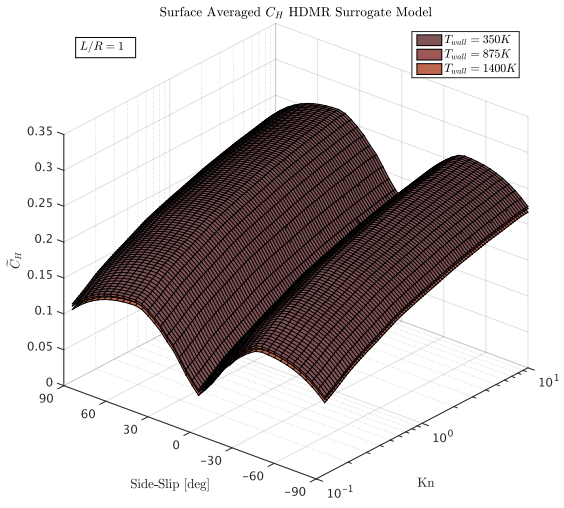

Figure 14. Cylinder $\widetilde{\mathbb{C}}_{\mathbb{H}}$ iso-surfaces for the T_{wall}, generated by extending the dataset to a wider range of α by employing the axial-symmetry condition. The figure shows the small weight of an input with a low sensitivity variance index.

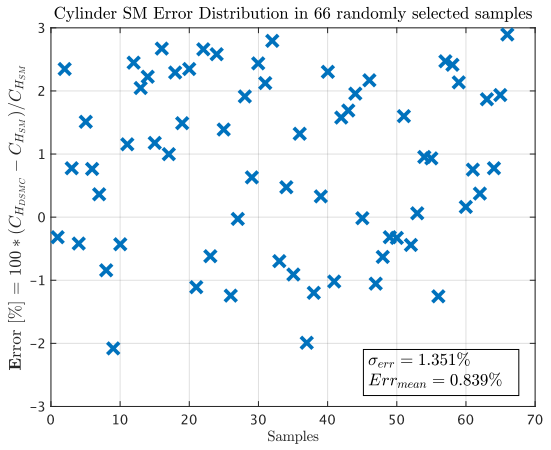

Figure 15. Cylinder $\widetilde{\mathbb{C}}_{\mathbb{H}}$ error distribution for 66 randomly generated samples within the validity intervals (Table 2).

specific DSMC mesh refinement correction factor has been evaluated. The correction factor, defined as the ratio between a high-accuracy and a low-accuracy DSMC surface-averaged results, has been proven to be a good compromise between accuracy and computational efficiency when a high number of DSMC simulation on the same shape is expected. Such a corrective coefficient requires an initial number of simulation to be calibrated. It has been shown that the difference between the high-fidelity and low-fidelity DSMC setup results increases as the Knudsen number decreases toward the slip-flow regime.

In the future it is planned to develop a better and wider surrogate model for a parameterized parallelepiped, thus to be usable for a wide range of simple-shaped geometries. In addition, the current surrogate models will be extended toward the Free Molecular regime. The surrogate models will be implemented in a lumped mass ablation module within FOSTRAD. Moreover, the current work has built the foundations for developing a local surface heat transfer mapping for parameterized geometries. In fact, the C_H averaging post-processing method is based on reading the local surface heat transfer. Currently, a methodology to interpolate and approximate the normalized heat transfer maps is being researched and aims at introducing a coupled flow-structure 3D thermal ablation module within FOSTRAD.

ACKNOWLEDGMENTS

The authors would like to state that the results were obtained using the EPSRC funded ARCHIE-WeSt High Performance Computer (www.archie-west.ac.uk). EPSRC grant no. EP/K000586/1.

REFERENCES

1. Bird, G.: Definition of mean free path for real gases. Physics of Fluids (1958-1988) **26**(11), 3222–3223 (1983)
2. Borgnakke, C., Larsen, P.S.: Statistical collision model for monte carlo simulation of polyatomic gas mixture. Journal of computational Physics **18**(4), 405–420 (1975)
3. Fritsch, F.N., Carlson, R.E.: Monotone piecewise cubic interpolation. SIAM Journal on Numerical Analysis **17**(2), 238–246 (1980)
4. Hirschfelder, J.O., Curtiss, C.F., Bird, R.B., Mayer, M.G.: Molecular theory of gases and liquids, vol. 26. Wiley New York (1954)
5. Kemp, N.H., Riddel, F.R.: Heat transfer to satellite vehicles re-entering the atmosphere. Journal of Jet Propulsion **27**(2), 132–137 (1957)
6. Koppenwallner, G., Fritsche, B., Lips, T., Klinkrad, H.: Scarab-a multi-disciplinary code for destruction analysis of space-craft during re-entry. In: Fifth European Symposium on Aerothermodynamics for Space Vehicles, vol. 563, p. 281 (2005)
7. Kubicek, M., Minisci, E., Cisternino, M.: High dimensional sensitivity analysis using surrogate modeling and high dimensional model representation. International Journal for Uncertainty Quantification **5**(5) (2015)
8. Lips, T., Fritsche, B.: A comparison of commonly used re-entry analysis tools. Acta Astronautica **57**(2), 312–323 (2005)
9. Mehta, P., Minisci, E., Vasile, M., Walker, A.C., Brown, M.: An open source hypersonic aerodynamic and aerothermodynamic modelling tool. In: 8th European Symposium on Aerothermodynamics for Space Vehicles (2015)
10. Mehta, P.M., Walker, A., Brown, M., Minisci, E., Vasile, M.L.: Sensitivity analysis towards probabilistic re-entry modeling of spacecraft and space debris. In: AIAA Modeling and Simulation Technologies Conference, p. 3098 (2015)
11. Picone, J.M., Heding, A.E., Drob, D.P., Aikin, A.C.: Nrlmsise00 empirical model of the atmosphere: Statistical comparisons and scientific issues. Journal of Geophysical Research: space Physics **107**(A12) (2002)
12. Rochelle, W.C., Kinsey, R.E., Reid, E.A., Reynolds, R.C., Johnson, N.L.: Spacecraft orbital debris reentry: Aerothermal analysis (1997)
13. Scanlon, T.J., Roohi, E., White, C., Darbandi, M., Reese, J.M.: An open source, parallel dsmc code for rarefied gas flows in arbitrary geometries. Computers And Fluids **39**(10), 2078–2089 (2010)
14. Scanlon, T.J., White, C., Borg, M.K., Palharini, R.C., Farbar, E., Boyd, I.D., Reese, J.M., Brown, R.E.: Open-source direct simulation monte carlo chemistry modeling for hypersonic flows. AIAA Journal **53**(6), 1670–1680 (2015)
15. Schaaf, S., Chambre, P.: Flow of rarefied gases, high speed aerodynamics and jet propulsion, vol. iv, sect. 8 (1957)
16. Sun, Z.X., Tang, Z., He, Y.L., Tao, W.Q.: Proper cell dimension and number of particles per cell for dsmc. Computers & Fluids **50**(1), 1–9 (2011)